mTOR hyperactivity mediates the detrimental effects of a high sucrose diet on Alzheimer's disease pathology

Miranda E. Orr[1], **Angelica Salinas**[1], **Rochelle Buffenstein**[1], and **Salvatore Oddo**[1,2,*]

[1]Department of Physiology and The Barshop Institute for Longevity and Aging Studies, University of Texas Health Science Center at San Antonio. San Antonio, TX

[2]Banner Sun Health Research Institute, Sun City, AZ and Department of Basic Medical Sciences, University of Arizona College of Medicine-Phoenix, Phoenix AZ

Abstract

High sugar consumption and diabetes increase the risk of developing Alzheimer's disease (AD) by unknown mechanisms. Using an animal model of AD, here we show that high sucrose intake induces obesity with changes in central and peripheral insulin signaling. These pre-diabetic changes are associated with an increase in Aβ production and deposition. Moreover, high sucrose ingestion exacerbates tau phosphorylation by increasing Cdk5 activity. Mechanistically, the sucrose-mediated increase in AD-like pathology is due to hyperactive mTOR, a key nutrient sensor important in regulating energy homeostasis. Specifically, we show that rapamycin, an mTOR inhibitor, prevents the detrimental effects of sucrose in the brain without altering changes in peripheral insulin resistance. Overall, our data suggest that high sucrose intake and dysregulated insulin signaling, which are known to contribute to the occurrence of diabetes, increase the risk of developing AD by upregulating mTOR signaling. Therefore, early interventions to modulate mTOR activity in individuals at high risk of developing diabetes may decrease their AD susceptibility.

Keywords

Aβ; amyloid-β; APP; tau; tangles; insulin resistance; diabetes

Introduction

Alzheimer's disease (AD) is an untreatable neurodegenerative disorder currently affecting more than 5 million Americans. The vast majority of AD cases are sporadic and of unknown etiology; nevertheless, epidemiological studies have provided crucial insight into disease risk factors (Mayeux and Stern, 2012). Growing evidence shows that certain lifestyle choices, such as a high sugar or high fat diet, increase the risk of developing AD (Biessels,

et al., 2006). The Rotterdam study, a historic prospective population-based longitudinal study, identified that diabetes alone increases the risk of developing AD by ~2 fold (Ott, et al., 1999); this finding has been widely confirmed (reviewed by (Sims-Robinson, et al., 2010). Treating midlife health conditions known to increase the risk for developing AD, such as diabetes, may provide an opportunity for managing the projected increase in AD incidence.

Clinically, type 2 diabetic (T2D)/metabolic syndrome and AD patients share many common pathophysiological features. These include hyperglycemia, hyperinsulinemia, insulin resistance, glucose intolerance, dyslipidemia and inflammation; these traits reportedly correlate with attention and memory deficits (Jones, et al., 2009). Mounting evidence suggests that insulin resistance and concomitant elevated blood glucose is a key metabolic dysfunction contributing to AD (reviewed by (Cholerton, et al., 2013)). Namely, recent studies have reported evidence for insulin resistance in AD brains independent of the patients' diabetic status (e.g., (Talbot, et al., 2012)). Additionally, preliminary results from an on-going clinical study have revealed that T2D patients taking the insulin sensitizing drug, metformin, were less likely to develop AD then T2D patients taking other anti-diabetic medications (ClinicalTrials.gov Identifier: NCT01595646).

Neuropathologically, the AD brain is characterized by the accumulation of plaques, comprised mainly of amyloid-β (Aβ), and neurofibrillary tangles that are largely formed of hyperphosphorylated protein tau (Querfurth and LaFerla, 2010). Notably, patients with T2D have increased levels of hyperphosphorylated tau in their brains (Liu, et al., 2009), further strengthening the link between diabetes and AD. The use of AD mouse models with either genetically or chemically induced-diabetes have also reported a link between diabetes and AD pathologies (Jolivalt, et al., 2010; Ke, et al., 2009; Plaschke, et al., 2010; Takeda, et al., 2010). For example, inducing type I diabetes by streptozotocin (STZ) exacerbated the development of neurofibrillary tangles in a mouse model overexpressing mutant human tau (Ke, et al., 2009). Similarly, induction of experimental diabetes with STZ or analogous drugs increased Aβ and tau levels in wild type mice and rabbits (Bitel, et al., 2012; Ke, et al., 2009). Collectively, these studies provide compelling evidence that these prevalent age-associated diseases share alterations in common molecular pathways associated with glucose metabolism. However, the molecular mechanisms underlying the link between abnormal glucose homeostasis and AD remain to be elucidated.

mTOR is a protein kinases that plays a key role in maintaining energy homeostasis in the brain and other tissue types (Mannaa, et al., 2013). As an energy sensor, mTOR regulates numerous cellular pathways including protein translation, cell growth and proliferation. To modulate insulin signaling in times of high nutrient exposure, mTOR directly phosphorylates the insulin receptor leading to its internalization; this, in turn, results in a decrease of mTOR signaling (Wullschleger, et al., 2006). However, through the same mechanisms, chronic mTOR hyperactivity leads to insulin resistance, a key feature of T2D (Saha, et al., 2011). mTOR hyperactivity is also found in AD brains and in AD mouse models (Caccamo, et al., 2010; Caccamo, et al., 2011; Oddo, 2012; Pei and Hugon, 2008). We, and others, have shown that restoring mTOR activity using an mTOR inhibitor, rapamycin, mitigates AD-associated pathology and cognitive deficits (Caccamo, et al., 2010; Majumder, et al., 2012; Majumder, et al., 2011; Spilman, et al., 2010). As mTOR hyperactivity is common to both diabetes and AD, here, we explored the role of mTOR signaling as a molecular link between these two agerelated diseases.

Results

Prolonged sucrose intake alters insulin signaling in 3xTg-AD mice

To better understand the relation among AD, insulin resistance and diabetes we used a candidate approach and focused on the role of mTOR signaling, given its involvement in AD pathogenesis, energy homeostasis and insulin signaling. Specifically, 12-month-old 3xTg-AD mice, a widely used animal model of AD, were randomly assigned to one of the following groups: (i) 15 mice had ad libitum access to 20% sucrose water as the only source of water, these mice will be referred to as 3xTg-AD^{Suc} here thereafter; (ii) 15 mice had ad libitum access to regular water, these mice will be referred to as 3xTg-AD^{CTL} here thereafter; (iii) 15 mice had ad libitum access to 20% sucrose water as the only source of water plus rapamycin-enriched food, these mice will be referred to as 3xTg-AD$^{Suc+Rapa}$ here thereafter (Fig. 1A). The mTOR inhibitor, rapamycin, was added to the food as previously described (Harrison, et al., 2009). Mice were kept on their respective diets for 12 weeks.

One week after commencing the sucrose supplementation either with (3xTg-AD$^{Suc+Rapa}$) or without (3xTg-AD^{Suc}) rapamycin treatment, both mouse cohorts began gaining more weight than 3xTg-AD^{CTL} mice. While the 3xTg-AD^{CTL} mice gained 1% body mass during the first week, 3xTg-AD^{Suc} and 3xTg-AD$^{Suc+Rapa}$ mice gained 5% and 7% body mass, respectively (Fig. 1B). All mice receiving sucrose-supplemented water continued to gain weight throughout the experiment with a final weight gain of 28% in 3xTg-AD^{Suc} and 35% in 3xTg-AD$^{Suc+Rapa}$ compared to a 6% weight gain in 3xTg-AD^{CTL} mice (p<0.0001; Fig. 1B–C). 3xTg-AD$^{Suc+Rapa}$ mice gained significantly more weight than 3xTg-AD^{Suc} mice at many of the biweekly weight measurements (as indicated by Tukey post hoc analysis); however their final weights did not significantly differ (Fig. 1B–C).

To assess whether this change in weight was due to increased lean or fat mass, we measured body composition using dual-energy X-ray absorptiometry (DEXA) at the end of the treatment. DEXA scanning revealed that 3xTg-AD^{Suc} and 3xTgAD$^{Suc+Rapa}$ mice had gained comparable amounts of lean mass, which was significantly higher than 3xTg-AD^{CTL} mice (13% and 11%, respectively; p<0.01; Fig. 1D). We also found that the amount of fat mass was significantly different among the three groups (p < 0.001). The two cohorts receiving sucrose supplementation, 3xTg-AD^{Suc} and 3xTg-AD$^{Suc+Rapa}$ mice had 64% and 87% greater fat mass composition than 3xTg-AD^{CTL} mice (p < 0.001 and p < 0.0001, respectively). Though additional supplementation with rapamycin resulted in 23% greater fat mass than sucrose alone, the increase did not reach significance. (p = 0.27; Fig. 1D).

During the course of the study, both mouse cohorts receiving sucrose water required frequent bedding changes due to excess urination indicative of a sugar-induced osmotic diuresis. To confirm this anecdotal observation, we conducted a spot urinalysis after 8 weeks of treatment. We found that the urine specific gravity (1.025, 1.012 and 1.015 for 3xTg-AD^{CTL}, 3xTg-AD^{Suc} and 3xTg-AD$^{Suc+Rapa}$ mice, respectively) was significantly different among the three groups (p < 0.0001) with both sucrose-treated groups showing significantly more dilute urine than 3xTg-AD^{CTL} mice (p < 0.001; Fig 1E). The urine specific gravity was not statistically significant between 3xTg-AD^{Suc} and 3xTg-AD$^{Suc+Rapa}$ mice (Fig. 1E). Notably, urine from three of the 3xTg-AD$^{Suc+Rapa}$ mice contained detectable amounts of ~2.5 mg/ml of glucose indicating that the renal threshold for glucose absorption was exceeded and that animals exhibited some manifest diabetes-like symptoms. Glucose was not found in the urine of any other mouse.

To determine whether prolonged sucrose supplementation had altered endocrine regulation of glucose metabolism, we conducted a fasting glucose tolerance test (GTT), a commonly used diagnostic test for prediabetic states of insulin resistance and diabetes (Ye, et al., 2012).

Specifically, mice were fasted 16 hours overnight and then received a single intraperitoneal (i.p.) injection of 2 g/kg of sucrose (3xTg-AD^{CTL} n=11; 3xTg-AD^{Suc} n=8; 3xTg-AD$^{Suc+Rapa}$ n=7). To remove the confounding effects of stress-induced handling and obtain control values, an equal number of mice per group received a single i.p. injection of PBS. Serum glucose levels were measured before the i.p. injection and then again every 15 minutes post injection for the first hour, and every 30 minutes for the second hour with the final measurement at 215 minutes post injection. We found that fasting blood glucose levels were comparable among the three groups (77+/− 4mg/dL for 3xTg-AD^{Suc} mice; 77 +/− 3 mg/dL for 3xTg-AD$^{Suc+Rapa}$ mice; 73 +/− 3 mg/dL for 3xTg-AD^{CTL} mice; Fig. 1F). Likewise, peak blood glucose levels were similar among the three groups (449 +/− 19 mg/dL, 446 +/− 21 mg/dL and 444 +/− 23 mg/dL, for 3xTg-AD^{Suc}, 3xTg-AD$^{Suc+Rapa}$ and 3xTg-AD^{CTL} mice, respectively). However, we found that 3xTg-AD^{Suc} and 3xTg-AD$^{Suc+Rapa}$ mice displayed impairments in their ability to restore the elevated blood glucose levels back to baseline. Toward this end, blood glucose levels from 3xTg-AD^{CTL} mice subject to the GTT peaked 30 minutes after the glucose bolus and returned to baseline levels within 120 minutes (Fig 1F). These data are consistent with what is reported in other laboratory mice (Jimenez-Palomares, et al., 2012). In contrast, blood glucose levels of 3xTg-AD^{Suc} and 3xTg-AD$^{Suc+Rapa}$ mice continued to rise for longer and peaked at 45 minutes. More strikingly, in both sucrose supplemented groups, blood glucose levels remained significantly higher than baseline (i.e. 3xTg-AD injected with PBS, 3xTg-AD$^{CTL-PBS}$) for over two hours and returned back to baseline only at 215 minutes. In other words, we found that while the 3xTg-AD^{CTL} mice had, within 2 hours, restored their blood sugar back to levels comparable to 3xTg-AD$^{CTL-PBS}$ mice, blood glucose levels from 3xTg-AD^{Suc} and 3xTg-AD$^{Suc+Rapa}$ mice remained over three-times higher than 3xTg-AD$^{CTL-PBS}$ (259 +/− 40 mg/dL and 300 +/− 33 mg/dL, respectively) at the same time point. Indeed blood glucose levels of 3xTg-AD^{Suc} and 3xTg-AD$^{Suc+Rapa}$ mice were significantly different than the 3xTg-AD^{CTL} mice at measurements from 45 minutes through 120 minutes (3xTg-AD$^{Suc+Rapa}$: $p < 0.01$ at 45 minutes, $p < 0.05$ at 60 minutes, and $p < 0.0001$ for each measurement thereafter; 3xTg-AD^{Suc}: $p<0.01$ at 45 minutes and $p<0.0001$ at 90 and 120 minutes). The area under the curve (AUC) of a glucose tolerance test provides a better assessment of glucose tolerance. AUC analysis revealed that glucose tolerance was significantly different among the three groups (One-way ANOVA; $p = 0.003$ Fig. 1G) with both 3xTg-AD^{Suc} and 3xTg-AD$^{Suc+Rapa}$ cohorts showing significantly higher AUCs relative to 3xTg-AD^{CTL} mice ($p = 0.04$ and $p = 0.001$, respectively; Fig. 1G). Collectively, these data indicate that 3 months of sucrose supplementation induced alterations in insulin signaling in 3xTg-AD^{Suc} and 3xTg-AD$^{Suc+Rapa}$ mice.

High sucrose intake induced aberrant central insulin and mTOR signaling

To investigate the effects of high sucrose intake on brain insulin signaling, we measured the levels of total and phospho insulin receptor substrate 1 (IRS-1). IRS-1 is an intracellular adaptor protein and key regulator of insulin signaling; in response to insulin, IRS-1 becomes phosphorylated at selective tyrosine residues and recruits intracellular signal-transducing molecules to perpetuate the insulin signal (Backer, et al., 1992; Myers, et al., 1992). However, IRS-1 phosphorylation at serine residues can positively or negatively regulate insulin signaling depending on the residue(s) phosphorylated (reviewed by (Tanti and Jager, 2009). For example, phosphorylation at Tyr 608 always facilitates insulin signaling while phosphorylation of the serine residues 318 can either facilitate or inhibit insulin signaling, depending on the protein kinase doing the phosphorylation (Copps and White, 2012). Further, phosphorylation at Ser 612 is always inhibitory, disrupts insulin signaling and contributes to insulin resistance (Tanti and Jager, 2009).

We found that the steady-state levels of total IRS-1 were significantly different among the three groups (p < 0.0001) with 3xTg-AD[Suc] mice displaying significantly higher levels than 3xTg-AD[CTL] and 3xTg-AD[Suc+Rapa] mice (p < 0.0001 and p = 0.0005, respectively; Fig. 2A–B). Additionally, we found that the levels of IRS-1 phosphorylated at serine 318 and 612 were significantly different among groups (p=0.034 and p=0.0027, respectively). Post-hoc analysis indicated that the steady-state levels of IRS-1 phosphorylated at serine 318 were significantly higher in 3xTgAD[Suc] than 3xTg-AD[CTL] mice (p=0.0265; Fig. 2A–B). Additionally, we found that the IRS-1 levels phosphorylated at serine 612 were significantly higher in the brains of 3xTg-AD[Suc] mice than 3xTg-AD[CTL] and 3xTg-AD[Suc+Rapa] mice (p = 0.0044 and p = 0.01; Fig. 2A–B). Finally, we found that the levels of IRS-1 phosphorylated at Tyr 608 were significantly increased by sucrose and such an increase was prevented by rapamycin (p = 0.0173; Fig. 2A–B). These results clearly show that sucrose intake altered central IRS-1 signaling, which was prevented by rapamycin.

To dissect the mechanism by which rapamycin prevented the sucrose mediated changes in insulin signaling, we measured brain mTOR activity and signaling. A widely used method for assessing mTOR activity is by measuring the steady-state levels of downstream targets directly phosphorylated by mTOR, such as p70S6K phosphorylated by mTOR at threonine 389, and 4EBP1 phosphorylated by mTOR at threonine 37/46. Total mTOR protein levels were comparable among all mice (Fig. 2C). In contrast, we found that the levels of mTOR phosphorylated at serine 2448 were significantly different among the three groups (p = 0.0061). Phospho-mTOR levels were significantly higher in the 3xTg-AD[Suc] mice than 3xTg- AD[CTL] and 3xTg-AD[Suc+Rapa] mice (p = 0.01 and p = 0.007; Fig. 2C–D). Additionally, we found that total levels of p70S6K were similar among the three groups, while the 3xTg-AD[Suc] mice had significantly higher phospho-p70S6K than 3xTg-AD[CTL] and 3xTg-AD[Suc+Rapa] mice (p = 0.0203 and p < 0.0001, respectively). Finally, we found that total and phospho-4EBP1 levels, which reportedly are less responsive to rapamycin treatment and mTOR hyperactivity (Choo, et al., 2008), were similar among the three groups (Fig. 2C–D). These results clearly show that sucrose intake increased central mTOR activity and signaling, while rapamycin prevented these changes.

Rapamycin mitigates the effect of sucrose intake on Aβ and tau pathology

All mice were 15-months-old at the end of the treatment when sacrificed. At this age, 3xTg-AD mice display phenotypes consistent with early stage AD, including elevated Aβ with sparse plaques, and early tau phosphorylation and mislocalization (Oddo, et al., 2003; Oddo, et al., 2008). Aβ arises through sequential proteolytic cleavage of the transmembrane holoprotein amyloid precursor protein (APP). Cleavage of APP by β-site APP cleaving enzyme-1 (BACE-1) or α-secretase generates membrane associated APP C-terminal fragments referred to as C99 and C83, respectively. Further cleavage of the C99 fragment by the γ-secretase enzyme complex liberates the amyloidogenic Aβ peptide (Querfurth and LaFerla, 2010).

To evaluate the effects of high sucrose on Aβ metabolism, we first measured the levels of APP holoprotein and the major APP C-terminal fragments in by Western blot using whole brain homogenate. Levels of APP holoprotein and C99 were higher in the 3xTg-AD[Suc] mice than 3xTg-AD[CTL+Rapa] (Fig. 3A–B). In contrast, C83 levels were similar among all groups (Fig. 3A–B). More important, APP levels in 3xTgAD[Suc+Rapa] mice were not statistically different from 3xTg-AD[CTL] mice. Specifically, rapamycin reduced the sucrose-induced APP increase in half from 38% to 19% (Fig. 3B). Additionally, rapamycin mitigated C99 production from a sucrose-induced 34% increase to levels comparable to 3xTg-AD[CTL] mice (Fig. 3C). To address the mechanism behind the sucrose-induced increase in C99 production, we measured BACE-1 protein levels and found that they were significantly different among groups (p = 0.0006). Tukey's post hoc analysis revealed that 3xTg-AD[Suc]

mice had significantly more BACE-1 than 3xTg-AD^{CTL} (p = 0.0004), and the increase was prevented by rapamycin (Fig. 3K).

To assess the effects of sucrose on Aβ brain deposition, we stained brain sections with an anti-Aβ$_{1–42}$ specific antibody and with Thioflavin S (Fig. 3D–I). Quantification of the Aβ staining revealed a striking >150% increase in hippocampal Aβ load in 3xTg-AD^{Suc} mice compared to 3xTg-AD^{CTL} mice (Fig. 3J), which is consistent with previous reports (Cao, et al., 2007). Impressively, rapamycin completely prevented such an increase as we found that the hippocampal Aβ accumulation was significantly lower in 3xTgAD$^{Suc+Rapa}$ mice than 3xTg-AD^{Suc} mice (p<0.005). Indeed, Aβ deposition was similar between 3xTgAD$^{Suc+Rap}$ and 3xTg-AD^{CTL} mice (Fig. 3D–J).

As the 3xTg-AD mice develop both Aβ and tau pathology, we were uniquely positioned to address the concomitant effects of sucrose on both pathologies. To determine the effects of sucrose on tau pathology, we first measured steady-state levels of the human tau by Western blot. We found that human tau levels were significantly higher in the 3xTg-AD^{Suc} and 3xTg-AD$^{Suc+Rapa}$ mice compared to 3xTg-AD^{CTL} mice (p < 0.001 and p< 0.005 respectively; Fig. 4A–B). Surprisingly, the effect of rapamycin on tau levels was modest and not sufficient to prevent the sucrose-mediated increase in tau levels. Toward this end, we found that in 3xTg-AD$^{Suc+Rapa}$ mice tau levels were still significantly higher than 3xTg-AD^{CTL} mice. We next probed for changes in tau phosphorylation, a stronger correlate to disease progression, using several phospho-specific tau antibodies: CP13 (which recognizes tau phosphorylated at serine 202), AT8 (which recognizes tau phosphorylated at serine 202 and threonine 205), PHF-1 (which recognizes tau phosphorylated at serine 396/404), and PG5 (which recognizes tau phosphorylated at serine 409). We found that levels of CP13 and AT8-positive tau were significantly higher in 3xTg-AD^{Suc} than in 3xTg-AD^{CTL} mice (p < 0.05; Fig. 4A, C). Notably, rapamycin administration prevented the sucrose-mediated increase in tau phosphorylation at serine 202 and threonine 205 as indicated by comparable CP13 and AT8 levels between 3xTg-AD^{CTL} and 3xTgAD$^{Suc+Rapa}$ (Fig. 4A, C). The sucrose-mediated increase in phospho-tau levels was selective as we found that sucrose increased PHF-1 and PG5 levels as well but these changes were not statistically significant (p = 0.4875 and p = 0.1164, respectively; Fig. 4A, D). To assess changes in tau conformation, we used the MC-1 antibody, which recognizes Nterminal amino acids 7–9 and C-terminal amino acids 312–322. We found a significant difference between 3xTg-AD^{Suc} and 3xTg-AD$^{Suc+Rapa}$ mice (p = 0.05; Fig 3C) indicating that rapamycin may alter mechanisms by which hyperphosphorylated tau adopts a pathogenic conformation. Indeed rapamycin treatment has proven efficacious in delaying disease onset in prion disease, the canonical protein misfolding disease (Cortes, et al., 2012).

To investigate brain regions most affected by tau phosphorylation, we measured tau deposition in histological sections. We found that that phospho-tau immunoreactivity was significantly higher in the dentate gyrus and CA1 regions of 3xTg-AD^{Suc} mice than the same brain regions in the 3xTg-AD^{CTL} mice (Fig. 4E–K). The dentate gyrus and CA1 are two subregions of the hippocampus that are highly affected by AD pathology in postmortem AD brains (Querfurth and LaFerla, 2010). Remarkably, rapamycin completely prevented the sucrosemediated effects on tau deposition; toward this end, we found that CP13- and AT8-positive immunoreactivity was similar between 3xTg-AD^{CTL} and 3xTg-AD$^{Suc+Rapa}$ mice (Fig. 4E–K).

Sucrose increased tau phosphorylation via a Cdk5-dependent mechanism

To explore the mechanism behind the sucrose-induced tau phosphorylation, we investigated levels of Cdk5 and GSK3β, two tau kinases heavily implicated in AD pathogenesis (reviewed by (Martin, et al., 2013). GSK3β activity is negatively regulated by

phosphorylation at residue serine 9 (Feng, et al., 2013; Stambolic and Woodgett, 1994). We found a non-significant increase in total and pSer9-GSK3β levels in all mice receiving sucrose-supplemented water (Fig. 5A–B). These findings suggest that GSK3β does not play a significant role in sucrose-induced tau phosphorylation. In agreement, we found that tau phosphorylation at serine 396/404, two amino acids phosphorylated by GSK3β (Augustinack, et al., 2002; Cavallini, et al., 2013), were not significantly different among groups (Fig. 4A, C).

Cdk5 requires association with p35 for its catalytic activation (Tang, et al., 1995; Tsai, et al., 1994; Utreras, et al., 2011; Zhu, et al., 2012) Proteolytic cleavage of p35 generates a smaller protein, p25, which also activates Cdk5 (Lew, et al., 1994). To determine if Cdk5 activity correlated with the tau hyperphosphorylation, we assayed brain levels of Cdk5, p35, and p25 by Western blot. While steady-state levels of Cdk5 and p25 were comparable among 3xTg-AD^{CTL}, 3xTg-AD^{Suc} and 3xTg-AD$^{Suc+Rapa}$ mice, we found that the p35 levels were significantly different among them (p = 0.04; Fig. 5A, C). Post-hoc analysis indicated that p35 levels were significantly higher in the brains of 3xTg-AD^{Suc} mice compared to 3xTg-AD^{CTL} and 3xTg-AD$^{Suc+Rapa}$ mice. Overall, p35 levels were 46% higher in the 3xTg-AD^{Suc} mice than 3xTg-AD^{CTL} mice. Such an increase was prevented by rapamycin. Notably, an increase in Cdk5-mediated phosphorylation is consistent with the tau phosphorylation data (Fig. 4); indeed, the tau residues found to be significantly elevated in 3xTg-AD^{Suc} mice (serine 202/205) are putative Cdk5 targets (Augustinack, et al., 2002; Cavallini, et al., 2013). In summary, while rapamycin did not completely prevent total tau or p35 upregulation and corresponding tau phosphorylation, it greatly mitigated the sucrose-induced pathogenic effects indicating that mTOR activation is necessary for the sucrose-induce tau phosphorylation.

Discussion

Currently there are no pharmacologic interventions that effectively cure, prevent, or delay AD progression. Midlife health conditions known to increase the risk for developing AD, such as diabetes, are treatable and may provide an opportunity for intervention. While many studies have independently confirmed an increased risk of AD and diabetes (reviewed by (Sims-Robinson, et al., 2010)), since the pivotal Rotterdam study was originally published in 1999, little progress has been made to understand the molecular pathways linking the diseases. In line with the observations from the Rotterdam report, we aimed to study the effects of a diet high in sugar on disease progression in middle-aged 3xTg-AD mice highly predisposed to develop ADlike pathology (Oddo, et al., 2003). Here we provide the first *in vivo* evidence that mTOR represents a mechanistic link between aberrant insulin signaling, obesity and AD.

Recent studies have revealed a role for rapamycin in altering insulin sensitivity in inbred C57BL/6 and heterogeneous mice (Fang, et al., 2013; Lamming, et al., 2013; Lamming, et al., 2012); however, we did not see such an effect. We found that, regardless of rapamycin intervention, all 3xTg-AD mice on sucrose developed peripheral insulin resistance as evidenced by abnormal GTT. Despite the presence of glucose in the urine of some mice, normal fasting blood glucose revealed that excess sugar intake over the 3 month period was not sufficient to induce type 2 diabetes. While all sucrose treated mice gained similar amounts of muscle mass, the fat mass in 3xTg-AD$^{Suc+Rapa}$ mice was 23% greater than in 3xTg-AD^{Suc} mice alone. Though this increase in fat mass did not reach significance, it is consistent with the role for mTOR signaling in adipose metabolism (reviewed by (Lamming and Sabatini, 2013)). Specifically, in cases of insulin resistance, mTORC1 activation alone is sufficient to initiate adipogenesis (Zhang, et al., 2009).

Though rapamycin administration did not prove efficacious in altering peripheral insulin resistance, we provide compelling evidence showing that reducing the sucrose-mediated mTOR hyperactivity in the brain has beneficial effects on brain insulin signaling and AD-like pathology. AD has been referred to as "type 3 diabetes", or "insulin resistance of the brain" (Steen, et al., 2005). Specifically, insulin receptor expression in human AD patients is inversely proportional to the Braak stage of AD progression (Rivera, et al., 2005; Steen, et al., 2005). Similarly, we found that 3xTg-AD^{Suc} mice expressed higher levels of phosphorylated IRS-1 at inhibitory and stimulatory residues suggesting, e.g., serine 318 and 612 and tyrosine 608, than 3xTg-AD^{CTL} mice suggesting IRS-1 dysregulation. Remarkably, reducing mTOR signaling was sufficient to prevent these changes; indeed, IRS-1 phosphorylation levels were comparable between control fed and 3xTg-AD$^{Suc+Rapa}$ mice. Overall, these finding suggest that mTOR plays a key role in regulating brain insulin signaling.

Remarkably, 3xTg-AD$^{Suc+Rapa}$ brain pathology and IRS-1 phosphorylation was not different from control fed mice; however, this mouse cohort was the most obese of the experimental groups and they exhibited a slightly, though non-significant, more impaired glucose tolerance. In essence, we found that the molecular changes in brain insulin signaling and mTOR function were uncoupled from the insulin sensitivity state of the periphery, clearly indicating that regulating insulin signaling in the periphery may not have the same effects on central insulin signaling. In keeping with this observation, a separate study showed that obesity-associated hyperinsulinemia did not alter peripheral glucose tolerance in weanling C57BL/6 mice fed high fat diet for 12–16 weeks, nor did it alter brain insulin signaling or tau phosphorylation (Becker, et al., 2012). Together these data suggest that in the presence of proper brain insulin signaling and mTOR activity, peripheral obesity and aberrant insulin signaling are not sufficient to exacerbate AD pathology. However, since mTOR is susceptible to these peripheral changes, as shown here, it may be an important mediator between health and disease and could provide an opportunity for therapeutic intervention.

Sucrose administration caused a significant increase in hippocampal Aβ plaque accumulation. 3xTg-AD^{Suc} mice displayed over 150% greater plaque deposition than mice on a control diet and provides some evidence that lifestyle, and in particular poor diet quality, may contribute significantly to the high incidence of AD as the American society, as a whole, becomes more obese. Impressively, reducing mTOR signaling completely abolished the sucrose-induced increase in plaque load. Consistent with this finding, we previously found that decreasing mTOR activity back to control levels ameliorated AD-like pathology (Caccamo, et al., 2013; Caccamo, et al., 2010; Majumder, et al., 2011). Mechanistically, we provide evidence that the increase in plaque accumulation was mediated by an increase in Aβ production. Toward this end, we found that the levels of full length APP as well as its BACE-1 cleavage product, C99, were significantly higher in 3xTg-AD^{Suc} mice than 3xTg-AD^{CTL} mice. Consistent with an increase in Aβ production, we also found that BACE-1 levels were higher in 3xTg-AD^{Suc} than 3xTg-AD^{CTL} mice. These results are highly consistent with a report showing that diabetes-induced increase in plaque load in 5xFAD mice correlated with elevated APP and BACE-1 levels (Devi, et al., 2012). Other studies are needed to determine why neither sucrose nor rapamycin had an effect on C83 levels.

Given that the 3xTg-AD mice develop both Aβ and tau pathology, we were uniquely positioned to determine the effects of sucrose on tau in parallel with changes in APP. We found that the high sucrose diet enhanced tau phosphorylation and induced pathological conformational changes, both of which correlate with AD pathogenesis (reviewed by (Binder, et al., 2005)). The Cdk5/p35 signaling pathway was of particular interest as it is

involved in pathogenicity of both AD and T2D. In AD Cdk5/p35 contributes to pathogenic tau phosphorylation, and in pancreatic beta cells p35 alters insulin secretion (Ubeda, et al., 2004). Mechanistically, we found that brains from all 3xTg-AD mice expressed comparable levels of tau kinase Cdk5, but sucrose induced an increase in levels of Cdk5 activator protein, p35. Indeed, Cdk5-mediated tau phosphorylation was significantly higher only in 3xTg-AD[Suc] mice with elevated p35, as indicated by increased phosphorylation at tau residues phosphorylated by Cdk5: serine 202/205. Consistently, glucose-induced p35 upregulation, and corresponding Cdk5/p35 activity, has been shown to increase in a glucose dose-dependent manner in pancreatic beta cells (Ubeda, et al., 2004). Notably, the increase in p35 levels, without a concomitant increase in p25 levels suggests that the effects of sucrose on p35 levels occur at production levels. Remarkably, rapamycin prevented the p35 upregulation and associated tau hyperphosphorylation indicating that it may be a previously uncharacterized mTOR-mediated process. Others have reported differences in GSK3β activity and corresponding tau phosphorylation following alterations in insulin signaling (Jolivalt, et al., 2010; Jolivalt, et al., 2008), which does not appear consistent with our finding. Sucrose did not increase in GSK3β- mediated tau phosphorylation as evidenced by unchanged serine 9 GSK3β phosphorylation, and similar levels of tau phosphorylation at GSK3β putative sites. As phosphorylation at GSK3β epitopes serine 396/404 coincides with advanced tau phosphorylation (Augustinack, et al., 2002), it is tempting to speculate that changes in GSK3β may have developed with a longer sucrose treatment.

In previous studies, we found that mTOR hyperactivity was linked to an increase in Aβ and tau pathology (Caccamo, et al., 2013; Caccamo, et al., 2010; Caccamo, et al., 2011; Majumder, et al., 2011). We also showed a direct link between mTOR and tau; indeed, genetically increasing mTOR signaling was sufficient to increase tau levels and phosphorylation (Caccamo, et al., 2013). These data, together with the results shown here, clearly indicate the primary role of mTOR signaling not only in AD but also in other tauopathies. Further, here we established that high sucrose intake was sufficient to induce mTOR hyperactivity, abnormal brain insulin signaling and exacerbate AD-like pathology in 15-month-old 3xTg-AD mice. Despite the marked peripheral insulin resistance and obesity in all sucrose-fed mice, they did not develop clinical diabetes over the three-month experiment. Our data strongly suggest that the insidious sucrose-induced metabolic syndrome evident in these mice accelerated the progression of AD-like pathology. Of great clinical relevance, we show that pharmacological intervention with an FDA-approved drug, rapamycin, abrogated the negative effects of sucrose on brain pathology, despite pre-existing peripheral insulin resistance and AD-predisposition. To our knowledge, this is the first study to provide *in vivo* evidence of a therapeutic that can alter the progression of AD-like pathology in response to aberrant insulin signaling. With the understanding that diabetics are twice as likely to develop AD as non-diabetics, currently 23 million Americans are highly susceptible to developing an untreatable neurodegenerative disease. Clinicians can readily test for insulin resistance and syndromes associated with glucose intolerance, and our data highlight the importance of intervention in individuals at the first sign of metabolic imbalance to reduce the risk of debilitating health and socioeconomic burden.

Methods

Mice

The 3xTg-AD mice used in these studies have been previously described (Oddo, et al., 2003); only female mice were used for this study. Mice were housed in 4–5 to cage. Twice weekly, fresh 20% sucrose dissolved in water was given to all 3xTg-AD[Suc] and 3xTgAD[Suc+Rapa] mice. Additionally, microencapsulated rapamycin (Harrison, et al., 2009) was added at a concentration of 14 mg/kg to mouse chow for 3xTgAD[Suc+Rapa] mice. 3xTg-

AD[CTL] mice were on regular water and regular chow. Mice were kept on their respective diets for 12 weeks, and body weight was determined twice weekly. All animal procedures were approved by The Institutional Animal Care and Use Committee of The University of Texas Health Science Center at San Antonio.

Urinalysis

Eight weeks after the beginning of the study, spot urine samples were taken from each mouse. Mice were scruffed and held over parafilm. Urination was stimulated by gently massaging their abdomens. Urine was transferred to eppendorf tubes and immediately placed on ice and stored at −80°C to maintain integrity prior to test. For urinalysis, samples were then thawed out at room temperature and analyzed with Multistix 10 SG reagent strips (Siemens).

GTT

The fasting glucose tolerance test was conducted eleven weeks after the beginning of the treatment. Mice were overnight fasted for 16 hours. At 4 pm the night prior to GTT, mice were transferred to clean cages with fresh water only; all food and sucrose water was removed. The following morning mice were weighed, and tails were nicked with a fresh razor blade for initial fasting blood glucose level. Half of the animals from each group received a glucose (2mg/kg) injection into the intraperitoneal (i.p.) cavity and the other half received an injection of PBS. Given that the concentration of the glucose stock was of 30 mg/ml, mice received between 226 and 475 μl of solution, based on their body weight. At 15, 30, 45, 60, 90, 120, and 215 minutes post-i.p. injection, blood glucose was sampled from the tail.

DEXA

Mice were weighed and anesthetized. A dual-energy X-ray absorptiometry (DEXA) scan was performed on each animal to acquire total lean and fat mass using a Lunar PIXImus Densiometer (GE Medical Systems). In order to ensure the readings were accurate, prior to mouse scanning a phantom scan was performed for DEXA calibration. We compared total mass as indicated by DEXA to that of a laboratory scale; measurements were within $1.64 \pm 1.25\%$ (average ± SD).

Biochemistry

Mice were anesthetized and transcardially perfused with ice cold PBS. Their brains were harvested, weighed, and sagittally bisected. One hemibrain was fixed for 48 hours in 4% paraformaldehyde for histological analyses and one hemibrain was frozen on dry ice for biochemical analyses. Frozen hemibrains were thawed slightly on ice and mechanically homogenized in ice-cold T-PER (Pierce) protein extraction buffer containing complete protease inhibitor (Roche) and phosphatase inhibitor (Invitrogen). Brain homogenates were untracentrifuged at 4C 100,000 g for 1 hour following a protocol that we have used in the past (e.g., (Medina, et al., 2011; Oddo, et al., 2007). The supernatant was used for Western blot analyses. Total protein concentration was determined using the bicinchoninic BCA assay (Pierce). 20 μg or proteins were loaded on 4–20% Tris-Glycine gels (Biorad) under reducing conditions and transferred to a nitrocellulose membrane at 50V for 2 hours. Membranes were incubated for 30 minutes in 5% bovine serum albumin (BSA) in TBST (0.1% Tween-20 in TBS pH 7.6) then incubated overnight in primary antibody. The blots were rinsed in TBST for 30 minutes then incubated in goat anti-mouse IRDye 680LT or goat anti-rabbit IRDye 800CW LICOR secondary antibodies (1:20,000) for 2 hours at room temperature. The membranes were rinsed for 30 minutes in TBST, 5 minutes in PBS, and imaged and analyzed using the LI-COR Odyssey. Protein densitometry was calculated by

dividing the integrated intensity (I.I. K counts) of the protein of interest by integrated intensity of β-Actin loading control. Primary antibodies: Rabbit anti: Total IRS-1, pIRS Ser612, pIRS Ser318, pIRS Tyr608, total and phospho-mTOR, total and phospho-p70S6K, total and phospho-4EBP1, total and phospho-GSK3β, BACE, Cdk5 and p35/p25 all used 1:1000 (Cell Signaling). Mouse anti-βActin (1:20,000, Millipore); HT7 (1:1000; Pierce); AT8 (1:200; Thermo Scientific); 22C11 (1:2000; Millipore). CP13, PHF1, PG5 and MC1 all used 1:200 generous gift from Peter Davies. CT15 antibody was a generous gift from Veronica Galvan.

Histology

For immunohistochemistry analysis, hemi-brains were fixed with 4% paraformaldehyde for 48 hr then transferred to 0.02% sodium azide solution in PBS until sectioned. Tissues were sectioned (50 μm thick) using a sliding vibratome, and stored in 0.02% sodium azide in PBS. The endogenous peroxidase activity was quenched with 3% H_2O_2 in 10% methanol for 30 min. For $A\beta_{1-42}$ staining tissue was fixed using ~95% formic acid (reagent grade>95%) for epitope retrieval for 7 min. Tissue was incubated overnight at 4°C with corresponding antibody. Sections were washed in Tris-buffered saline (TBS) to remove excess antibody and incubated in the appropriate secondary antibody for 1h at 20°C. Excess secondary antibody was washed and sections were developed with diaminobenzidine substrate using the avidin–biotin horseradish peroxidase system (Vector Labs, Burlingame, CA, USA). Primary antibodies [AT8 (1:1000) Thermo Scientific; $A\beta_{1-42}$ (1:200); CP13 (1:2000) generously donated by Peter Davies)]. For Thioflavin-S staining, tissues were mounted to slides, rinsed 3 times in 50% ethanol and placed in 1% Thioflavin-S (Sigma) for 10 minutes. Slides were sequentially rinsed 4 times each in 70% ethanol and 50% ethanol followed by a final rinse in water. Slides were coverslipped with Vectashield mounting medium (Vector Laboratories, Inc. Burlingame, CA). Images were obtained with a digital Zeiss camera and analyzed with ImageJ software. Quantification of staining was achieved using pixilation detection acquired by ImageJ. A threshold is set using a positive control and a standard mean gray area function, which allows the set software to recognize positive staining and decrease error caused by background staining.

Statistics

All data was analyzed using GraphPad Prism version 6.0c for Mac OS X, GraphPad Software, San Diego California, USA, www.graphpad.com. Data were analyzed by one or two way ANOVA followed by Tukey post-hoc analysis, when applicable.

Acknowledgments

References

Augustinack JC, Schneider A, Mandelkow EM, Hyman BT. Specific tau phosphorylation sites correlate with severity of neuronal cytopathology in Alzheimer's disease. Acta Neuropathol. 2002; 103(1):26–35. [PubMed: 11837744]

Backer JM, Myers MG Jr, Shoelson SE, Chin DJ, Sun XJ, Miralpeix M, Hu P, Margolis B, Skolnik EY, Schlessinger J, et al. Phosphatidylinositol 3'-kinase is activated by association with IRS-1 during insulin stimulation. EMBO J. 1992; 11(9):3469–3479. [PubMed: 1380456]

Becker K, Freude S, Zemva J, Stohr O, Krone W, Schubert M. Chronic peripheral hyperinsulinemia has no substantial influence on tau phosphorylation in vivo. Neurosci Lett. 2012; 516(2):306–310. [PubMed: 22521314]

Biessels GJ, Staekenborg S, Brunner E, Brayne C, Scheltens P. Risk of dementia in diabetes mellitus: a systematic review. Lancet Neurol. 2006; 5(1):64–74. [PubMed: 16361024]

Binder LI, Guillozet-Bongaarts AL, Garcia-Sierra F, Berry RW. Tau, tangles, and Alzheimer's disease. Biochim Biophys Acta. 2005; 1739(2–3):216–223. [PubMed: 15615640]

Bitel CL, Kasinathan C, Kaswala RH, Klein WL, Frederikse PH. Amyloid-beta and tau pathology of Alzheimer's disease induced by diabetes in a rabbit animal model. J Alzheimers Dis. 2012; 32(2): 291–305. [PubMed: 22785400]

Caccamo A, Magri A, Medina DX, Wisely EV, Lopez-Aranda MF, Silva AJ, Oddo S. mTOR regulates tau phosphorylation and degradation: implications for Alzheimer's disease and other tauopathies. Aging Cell. 2013; 12(3):370–380. [PubMed: 23425014]

Caccamo A, Majumder S, Richardson A, Strong R, Oddo S. Molecular interplay between mammalian target of rapamycin (mTOR), amyloid-beta, and Tau: effects on cognitive impairments. J Biol Chem. 2010; 285(17):13107–13120. [PubMed: 20178983]

Caccamo A, Maldonado MA, Majumder S, Medina DX, Holbein W, Magri A, Oddo S. Naturally secreted amyloid-beta increases mammalian target of rapamycin (mTOR) activity via a PRAS40-mediated mechanism. J Biol Chem. 2011; 286(11):8924–8932. [PubMed: 21266573]

Cao D, Lu H, Lewis TL, Li L. Intake of sucrose-sweetened water induces insulin resistance and exacerbates memory deficits and amyloidosis in a transgenic mouse model of Alzheimer disease. J Biol Chem. 2007; 282(50):36275–36282. [PubMed: 17942401]

Cavallini A, Brewerton S, Bell A, Sargent S, Glover S, Hardy C, Moore R, Calley J, Ramachandran D, Poidinger M, Karran E, Davies P, Hutton M, Szekeres P, Bose S. An unbiased approach to identifying tau kinases that phosphorylate tau at sites associated with Alzheimer disease. J Biol Chem. 2013; 288(32):23331–23347. [PubMed: 23798682]

Cholerton B, Baker LD, Craft S. Insulin, cognition, and dementia. Eur J Pharmacol. 2013

Choo AY, Yoon SO, Kim SG, Roux PP, Blenis J. Rapamycin differentially inhibits S6Ks and 4E-BP1 to mediate cell-type-specific repression of mRNA translation. Proc Natl Acad Sci U S A. 2008; 105(45):17414–17419. [PubMed: 18955708]

Copps KD, White MF. Regulation of insulin sensitivity by serine/threonine phosphorylation of insulin receptor substrate proteins IRS1 and IRS2. Diabetologia. 2012; 55(10):2565–2582. [PubMed: 22869320]

Cortes CJ, Qin K, Cook J, Solanki A, Mastrianni JA. Rapamycin delays disease onset and prevents PrP plaque deposition in a mouse model of Gerstmann-Straussler-Scheinker disease. J Neurosci. 2012; 32(36):12396–12405. [PubMed: 22956830]

Devi L, Alldred MJ, Ginsberg SD, Ohno M. Mechanisms underlying insulin deficiency-induced acceleration of beta-amyloidosis in a mouse model of Alzheimer's disease. PLoS One. 2012; 7(3):e32792. [PubMed: 22403710]

Fang Y, Westbrook R, Hill C, Boparai RK, Arum O, Spong A, Wang F, Javors MA, Chen J, Sun LY, Bartke A. Duration of rapamycin treatment has differential effects on metabolism in mice. Cell Metab. 2013; 17(3):456–462. [PubMed: 23473038]

Feng Y, Xia Y, Yu G, Shu X, Ge H, Zeng K, Wang J, Wang X. Cleavage of GSK-3beta by calpain counteracts the inhibitory effect of Ser9 phosphorylation on GSK-3beta activity induced by H(2)O(2). J Neurochem. 2013; 126(2):234–242. [PubMed: 23646926]

Harrison DE, Strong R, Sharp ZD, Nelson JF, Astle CM, Flurkey K, Nadon NL, Wilkinson JE, Frenkel K, Carter CS, Pahor M, Javors MA, Fernandez E, Miller RA. Rapamycin fed late in life extends lifespan in genetically heterogeneous mice. Nature. 2009; 460(7253):392–395. [PubMed: 19587680]

Jimenez-Palomares M, Ramos-Rodriguez JJ, Lopez-Acosta JF, Pacheco-Herrero M, Lechuga-Sancho AM, Perdomo G, Garcia-Alloza M, Cozar-Castellano I. Increased Abeta production prompts the onset of glucose intolerance and insulin resistance. Am J Physiol Endocrinol Metab. 2012; 302(11):E1373–E1380. [PubMed: 22414803]

Jolivalt CG, Hurford R, Lee CA, Dumaop W, Rockenstein E, Masliah E. Type 1 diabetes exaggerates features of Alzheimer's disease in APP transgenic mice. Exp Neurol. 2010; 223(2):422–431. [PubMed: 19931251]

Jolivalt CG, Lee CA, Beiswenger KK, Smith JL, Orlov M, Torrance MA, Masliah E. Defective insulin signaling pathway and increased glycogen synthase kinase-3 activity in the brain of diabetic mice: parallels with Alzheimer's disease and correction by insulin. J Neurosci Res. 2008; 86(15):3265–3274. [PubMed: 18627032]

Jones A, Kulozik P, Ostertag A, Herzig S. Common pathological processes and transcriptional pathways in Alzheimer's disease and type 2 diabetes. J Alzheimers Dis. 2009; 16(4):787–808. [PubMed: 19387113]

Ke YD, Delerue F, Gladbach A, Gotz J, Ittner LM. Experimental diabetes mellitus exacerbates tau pathology in a transgenic mouse model of Alzheimer's disease. PLoS One. 2009; 4(11):e7917. [PubMed: 19936237]

Lamming DW, Sabatini DM. A Central Role for mTOR in Lipid Homeostasis. Cell Metab. 2013

Lamming DW, Ye L, Astle CM, Baur JA, Sabatini DM, Harrison DE. Young and old genetically heterogeneous HET3 mice on a rapamycin diet are glucose intolerant but insulin sensitive. Aging Cell. 2013; 12(4):712–718. [PubMed: 23648089]

Lamming DW, Ye L, Katajisto P, Goncalves MD, Saitoh M, Stevens DM, Davis JG, Salmon AB, Richardson A, Ahima RS, Guertin DA, Sabatini DM, Baur JA. Rapamycin-induced insulin resistance is mediated by mTORC2 loss and uncoupled from longevity. Science. 2012; 335(6076): 1638–1643. [PubMed: 22461615]

Lew J, Huang QQ, Qi Z, Winkfein RJ, Aebersold R, Hunt T, Wang JH. A brain-specific activator of cyclin-dependent kinase 5. Nature. 1994; 371(6496):423–426. [PubMed: 8090222]

Liu Y, Liu F, Grundke-Iqbal I, Iqbal K, Gong CX. Brain glucose transporters, O-GlcNAcylation and phosphorylation of tau in diabetes and Alzheimer's disease. J Neurochem. 2009; 111(1):242–249. [PubMed: 19659459]

Majumder S, Caccamo A, Medina DX, Benavides AD, Javors MA, Kraig E, Strong R, Richardson A, Oddo S. Lifelong rapamycin administration ameliorates age-dependent cognitive deficits by reducing IL-1beta and enhancing NMDA signaling. Aging Cell. 2012; 11(2):326–335. [PubMed: 22212527]

Majumder S, Richardson A, Strong R, Oddo S. Inducing autophagy by rapamycin before, but not after, the formation of plaques and tangles ameliorates cognitive deficits. PLoS One. 2011; 6(9):e25416. [PubMed: 21980451]

Mannaa M, Kramer S, Boschmann M, Gollasch M. mTOR and regulation of energy homeostasis in humans. J Mol Med (Berl). 2013; 91(10):1167–1175. [PubMed: 23756767]

Martin L, Latypova X, Wilson CM, Magnaudeix A, Perrin ML, Yardin C, Terro F. Tau protein kinases: involvement in Alzheimer's disease. Ageing Res Rev. 2013; 12(1):289–309. [PubMed: 22742992]

Mayeux R, Stern Y. Epidemiology of Alzheimer disease. Cold Spring Harb Perspect Med. 2012; 2(8)

Medina DX, Caccamo A, Oddo S. Methylene blue reduces abeta levels and rescues early cognitive deficit by increasing proteasome activity. Brain pathology. 2011; 21(2):140–149. [PubMed: 20731659]

Myers MG Jr, Backer JM, Sun XJ, Shoelson S, Hu P, Schlessinger J, Yoakim M, Schaffhausen B, White MF. IRS-1 activates phosphatidylinositol 3'-kinase by associating with src homology 2 domains of p85. Proc Natl Acad Sci U S A. 1992; 89(21):10350–10354. [PubMed: 1332046]

Oddo S. The role of mTOR signaling in Alzheimer disease. Front Biosci (Schol Ed). 2012; 4:941–952. [PubMed: 22202101]

Oddo S, Caccamo A, Cheng D, Jouleh B, Torp R, LaFerla FM. Genetically augmenting tau levels does not modulate the onset or progression of Abeta pathology in transgenic mice. J Neurochem. 2007; 102(4):1053–1063. [PubMed: 17472708]

Oddo S, Caccamo A, Shepherd JD, Murphy MP, Golde TE, Kayed R, Metherate R, Mattson MP, Akbari Y, LaFerla FM. Triple-transgenic model of Alzheimer's disease with plaques and tangles: intracellular Abeta and synaptic dysfunction. Neuron. 2003; 39(3):409–421. [PubMed: 12895417]

Oddo S, Caccamo A, Tseng B, Cheng D, Vasilevko V, Cribbs DH, LaFerla FM. Blocking Abeta42 accumulation delays the onset and progression of tau pathology via the C terminus of heat shock protein70-interacting protein: a mechanistic link between Abeta and tau pathology. J Neurosci. 2008; 28(47):12163–12175. [PubMed: 19020010]

Ott A, Stolk RP, van Harskamp F, Pols HA, Hofman A, Breteler MM. Diabetes mellitus and the risk of dementia: The Rotterdam Study. Neurology. 1999; 53(9):1937–1942. [PubMed: 10599761]

Pei JJ, Hugon J. mTOR-dependent signalling in Alzheimer's disease. Journal of cellular and molecular medicine. 2008; 12(6B):2525–2532. [PubMed: 19210753]

Plaschke K, Kopitz J, Siegelin M, Schliebs R, Salkovic-Petrisic M, Riederer P, Hoyer S. Insulin-resistant brain state after intracerebroventricular streptozotocin injection exacerbates Alzheimer-like changes in Tg2576 AbetaPP-overexpressing mice. J Alzheimers Dis. 2010; 19(2):691–704. [PubMed: 20110613]

Querfurth HW, LaFerla FM. Alzheimer's disease. N Engl J Med. 2010; 362(4):329–344. [PubMed: 20107219]

Rivera EJ, Goldin A, Fulmer N, Tavares R, Wands JR, de la Monte SM. Insulin and insulin-like growth factor expression and function deteriorate with progression of Alzheimer's disease: link to brain reductions in acetylcholine. J Alzheimers Dis. 2005; 8(3):247–268. [PubMed: 16340083]

Saha AK, Xu XJ, Balon TW, Brandon A, Kraegen EW, Ruderman NB. Insulin resistance due to nutrient excess: is it a consequence of AMPK downregulation? Cell Cycle. 2011; 10(20):3447–3451. [PubMed: 22067655]

Sims-Robinson C, Kim B, Rosko A, Feldman EL. How does diabetes accelerate Alzheimer disease pathology? Nat Rev Neurol. 2010; 6(10):551–559. [PubMed: 20842183]

Spilman P, Podlutskaya N, Hart MJ, Debnath J, Gorostiza O, Bredesen D, Richardson A, Strong R, Galvan V. Inhibition of mTOR by rapamycin abolishes cognitive deficits and reduces amyloid-beta levels in a mouse model of Alzheimer's disease. PLoS One. 2010; 5(4):e9979. [PubMed: 20376313]

Stambolic V, Woodgett JR. Mitogen inactivation of glycogen synthase kinase-3 beta in intact cells via serine 9 phosphorylation. Biochem J. 1994; 303(Pt 3):701–704. [PubMed: 7980435]

Steen E, Terry BM, Rivera EJ, Cannon JL, Neely TR, Tavares R, Xu XJ, Wands JR, de la Monte SM. Impaired insulin and insulin-like growth factor expression and signaling mechanisms in Alzheimer's disease--is this type 3 diabetes? J Alzheimers Dis. 2005; 7(1):63–80. [PubMed: 15750215]

Takeda S, Sato N, Uchio-Yamada K, Sawada K, Kunieda T, Takeuchi D, Kurinami H, Shinohara M, Rakugi H, Morishita R. Diabetes-accelerated memory dysfunction via cerebrovascular inflammation and Abeta deposition in an Alzheimer mouse model with diabetes. Proc Natl Acad Sci U S A. 2010; 107(15):7036–7041. [PubMed: 20231468]

Talbot K, Wang HY, Kazi H, Han LY, Bakshi KP, Stucky A, Fuino RL, Kawaguchi KR, Samoyedny AJ, Wilson RS, Arvanitakis Z, Schneider JA, Wolf BA, Bennett DA, Trojanowski JQ, Arnold SE. Demonstrated brain insulin resistance in Alzheimer's disease patients is associated with IGF-1 resistance, IRS-1 dysregulation, and cognitive decline. J Clin Invest. 2012; 122(4):1316–1338. [PubMed: 22476197]

Tang D, Yeung J, Lee KY, Matsushita M, Matsui H, Tomizawa K, Hatase O, Wang JH. An isoform of the neuronal cyclin-dependent kinase 5 (Cdk5) activator. J Biol Chem. 1995; 270(45):26897–26903. [PubMed: 7592934]

Tanti JF, Jager J. Cellular mechanisms of insulin resistance: role of stress-regulated serine kinases and insulin receptor substrates (IRS) serine phosphorylation. Curr Opin Pharmacol. 2009; 9(6):753–762. [PubMed: 19683471]

Tsai LH, Delalle I, Caviness VS Jr, Chae T, Harlow E. p35 is a neural-specific regulatory subunit of cyclin-dependent kinase 5. Nature. 1994; 371(6496):419–423. [PubMed: 8090221]

Ubeda M, Kemp DM, Habener JF. Glucose-induced expression of the cyclin-dependent protein kinase 5 activator p35 involved in Alzheimer's disease regulates insulin gene transcription in pancreatic beta-cells. Endocrinology. 2004; 145(6):3023–3031. [PubMed: 14976144]

Utreras E, Terse A, Keller J, Iadarola MJ, Kulkarni AB. Resveratrol inhibits Cdk5 activity through regulation of p35 expression. Molecular pain. 2011; 7:49. [PubMed: 21736731]

Wullschleger S, Loewith R, Hall MN. TOR signaling in growth and metabolism. Cell. 2006; 124(3):471–484. [PubMed: 16469695]

Ye Y, Xie H, Zhao X, Zhang S. The oral glucose tolerance test for the diagnosis of diabetes mellitus in patients during acute coronary syndrome hospitalization: a meta-analysis of diagnostic test accuracy. Cardiovasc Diabetol. 2012; 11:155. [PubMed: 23270530]

Zhang HH, Huang J, Duvel K, Boback B, Wu S, Squillace RM, Wu CL, Manning BD. Insulin stimulates adipogenesis through the Akt-TSC2-mTORC1 pathway. PLoS One. 2009; 4(7):e6189. [PubMed: 19593385]

Zhu WL, Shi HS, Wang SJ, Xu CM, Jiang WG, Wang X, Wu P, Li QQ, Ding ZB, Lu L. Increased Cdk5/p35 activity in the dentate gyrus mediates depressive-like behaviour in rats. The international journal of neuropsychopharmacology / official scientific journal of the Collegium Internationale Neuropsychopharmacologicum. 2012; 15(6):795–809.
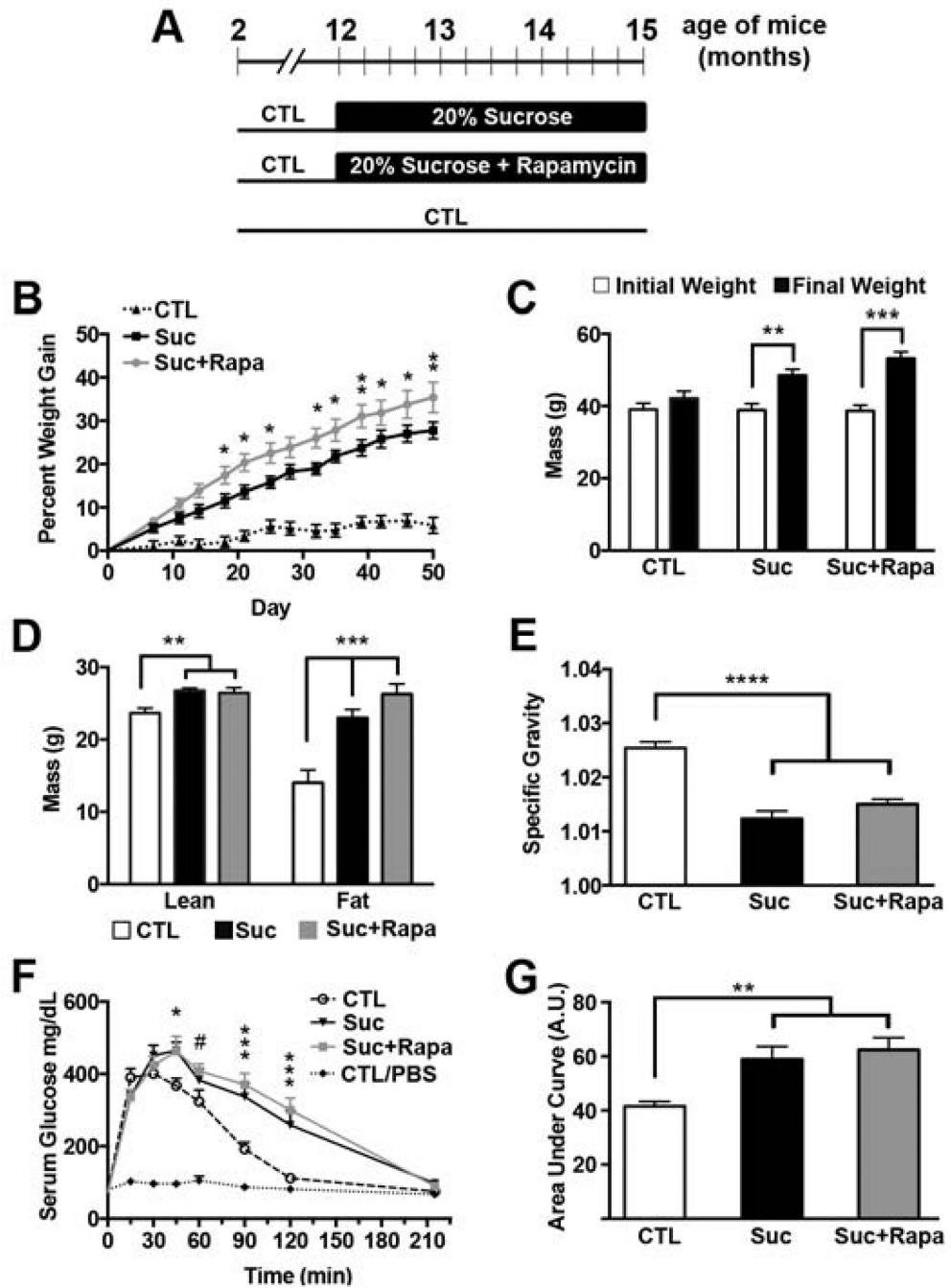
Figure 1. Sucrose-supplemented drinking water induced obesity, osmotic diuresis, and peripheral insulin resistance in 3xTg-AD mice

(A) Diagram of the experimental design. (B) All mice were weighed when they entered the study, one week after study commencement, and biweekly thereafter. Their weight change was calculated as the percent difference from day 0. 3xTg-AD$^{Suc+Rapa}$ gained significantly more weight than 3xTg-AD^{CTL} at every time point (day 7 $p<0.05$; day 11 $p<0.005$; and $p<0.0001$ each time point thereafter). 3xTg-AD^{Suc} gained significantly more weight than 3xTg-AD^{CTL} beginning at day 14 (day 14: $p<0.005$, $p<0.0001$ every time point thereafter). Asterisks indicate a significant difference between 3xTg-AD^{Suc} and 3xTg-AD$^{Suc+Rapa}$ groups (* $p < 0.05$; **$p < 0.005$). (C) The graph shows initial weight taken when mice

entered the study (day 0) and final weight at day 50. During the course of the study, 3xTg-AD[CTL] mice gained 6%, 3xTg-AD[Suc] mice gained 28% and 3xTg-AD[Suc+Rapa] gained 35% body mass (**$p<0.01$, ***$p<0.001$). (D) Fat mass and lean mass as measured by DEXA at the end of the study (* $p < 0.01$; ** $p<0.0005$; *** $p< 0.0001$). (E) Specific gravity (density of urine/density of water) measurements derived from spot urinalysis ($p<0.0001$). (F) Serum glucose concentrations during GTT, which was conducted after 11 weeks on the altered diet. Symbols indicate significant differences compared to 3xTg-AD[CTL]: # $p < 0.01$ and ### $p < 0.0001$ for both sucrose cohorts; * $p<0.05$ for only 3xTgAD[Suc+Rapa]. (G) Area under the curve for glucose was calculated using the trapezoid rule (** $p < 0.005$). A–E n=15 3xTg-AD[CTL], n=14 3xTg-AD[Suc+Rapa], n=14 3xTg-AD[Suc]; E–F: n=11 CTL 3xTg-AD[CTL]; n=4 CTL 3xTg-AD[CTL-PBS]; n=8 3xTg-AD[Suc]; n=7 3xTg-AD[Suc+Rapa]. Statistical analyses were performed by one-way ANOVA (D, E, G) or two-way ANOVA (B, C, F), followed by Tukey's multiple comparison test if $p < 0.05$. Results presented as means ± SEM.
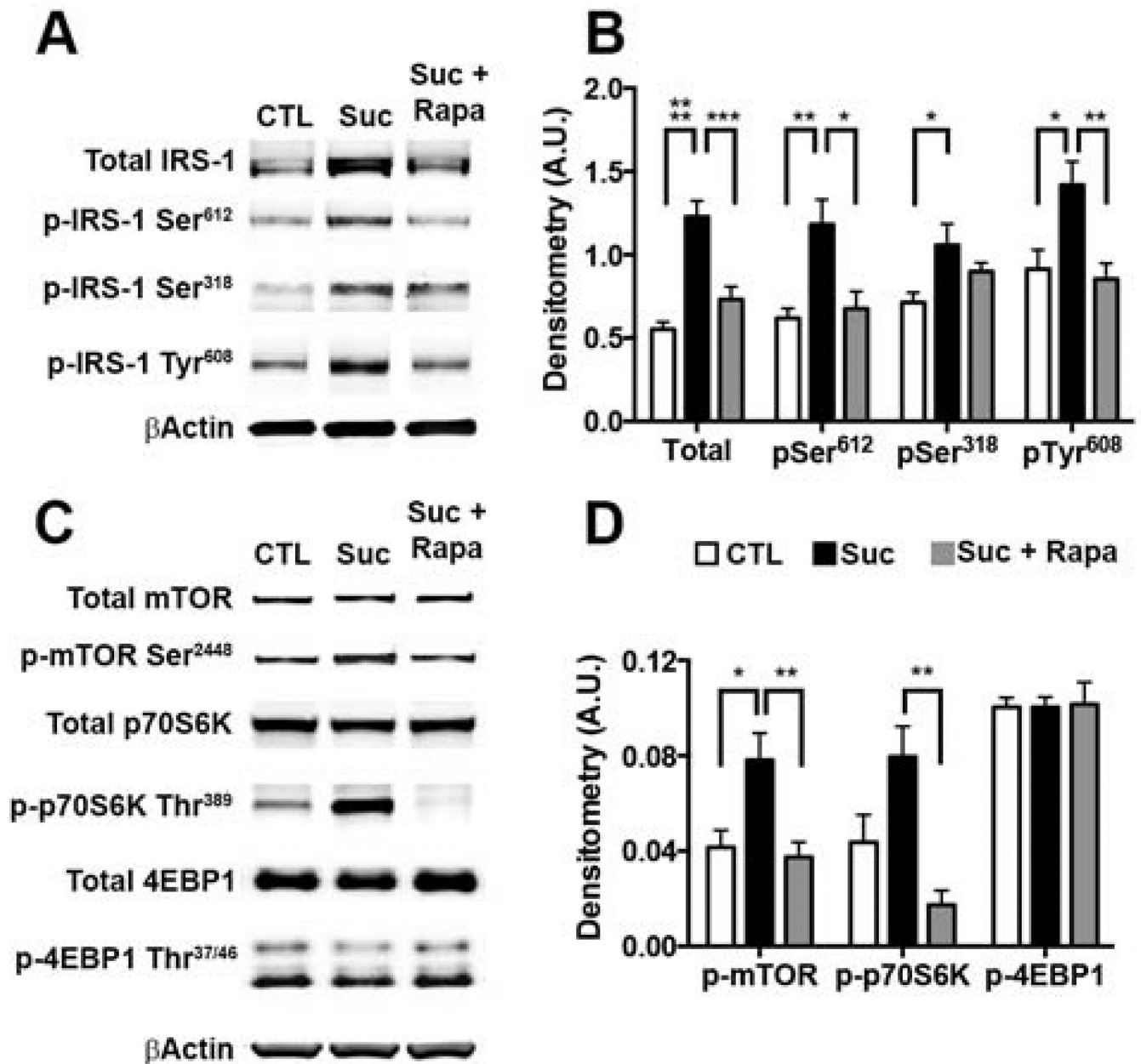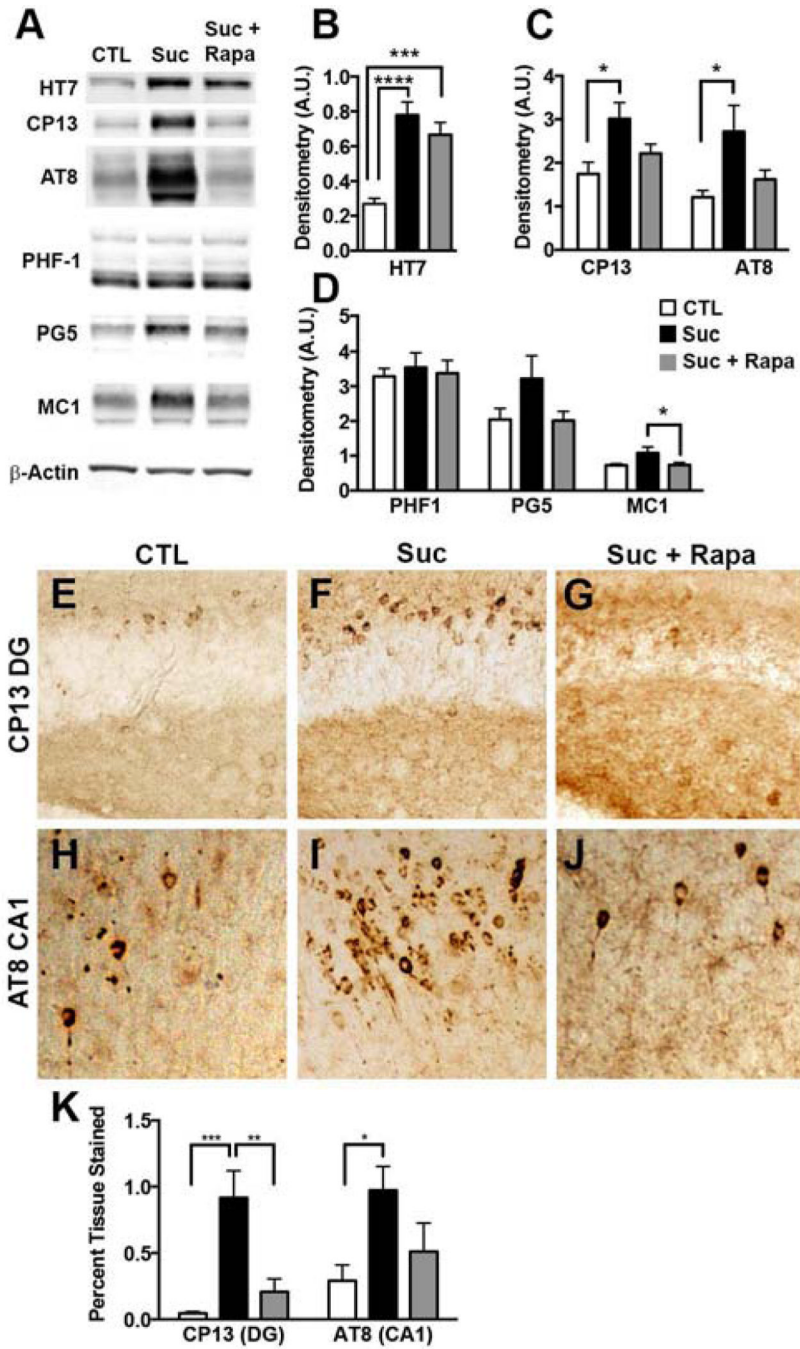
Figure 2. Sucrose-induced aberrant brain insulin is mediated by mTOR hyperactivity
Biochemical analyses were conducted on whole brain homogenates from 8 mice/group. (A)
Representative Western blots from brain proteins probed with the indicated antibodies. (B)
Relative protein level comparison by densitometric analyses. Data was generated by
normalizing IRS-1 protein of interest to β-Actin loading control (* $p < 0.05$; ** $p < 0.005$;
*** $p < 0.0005$; **** $p < 0.0001$). (C) Representative Western blots probed with the
indicated antibodies. (D) Denistometric analyses for mTOR signaling proteins normalized to
β-Actin loading controls (*$p < 0.05$; **$p < 0.01$; ***$p < 0.005$). Statistical analyses were
performed by ANOVA followed by Tukey's multiple comparison test if $p < 0.05$. Results
presented as means ± SEM.
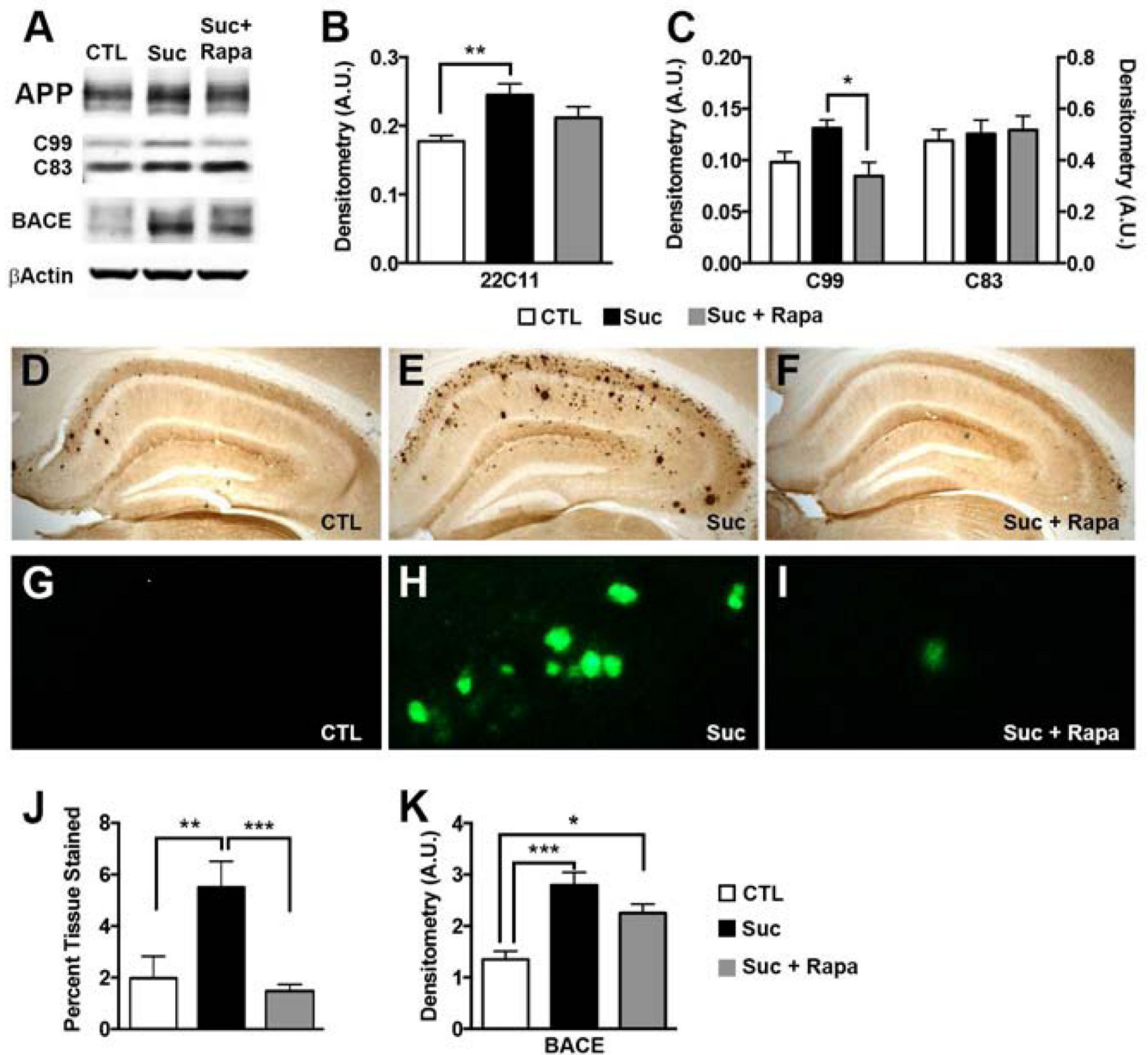
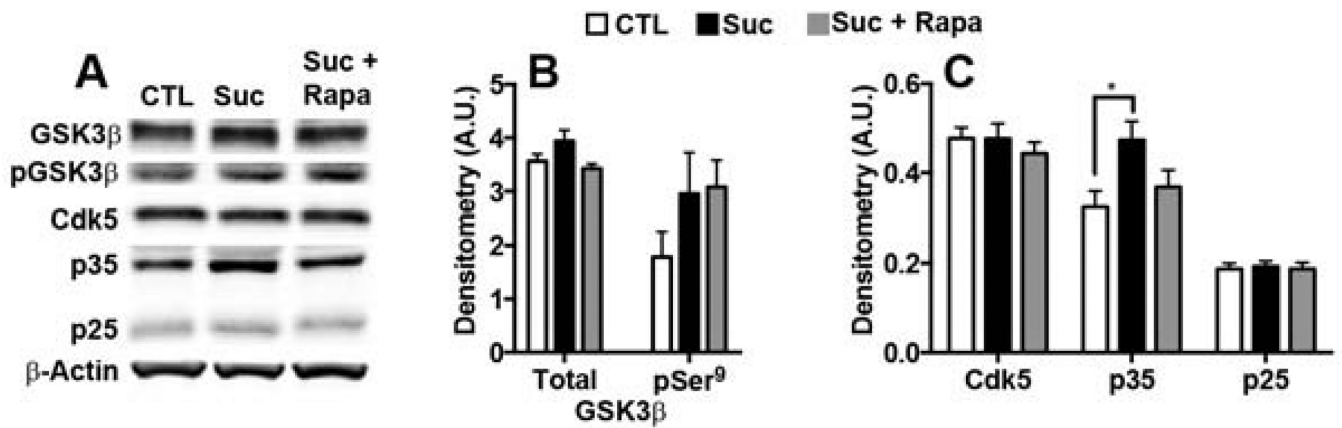**Figure 3. Sucrose enhanced Aβ pathology by an mTOR-mediated mechanism**
Biochemical analyses were conducted on whole brain homogenates from 8 mice/group. (A) Representative Western blots probed with the indicated antibodies. (B–C) Relative protein levels were quantified by densitometric analyses. The graphs were generated by normalizing the protein of interest to β-Actin loading control (*p < 0.05; ** p < 0.01). (D–F) Representative brain sections stained with a specific $A\beta_{1-42}$ antibody. (G–I) High magnification views of the hippocampal section shown in D–F stained with Thioflavin S. (J) Quantitative representation of percent hippocampal tissue stained by the $A\beta_{1-42}$ antibody (n=6; **p < 0.01). (K) Densitometric assessment of BACE-1 levels. Statistical analyses were performed by ANOVA followed by Tukey's multiple comparison test if p < 0.05. Results presented as means ± SEM.

Figure 4. Rapamycin prevented the sucrose-induced increase in tau levels and associated pathology

Biochemical analyses were conducted on whole brain homogenates from 8 mice/group. (A) Representative Western blots probed with the indicated antibodies. (B–D) Densitometry analyses of protein levels were obtained by normalizing the protein of interest to β-Actin loading control (* $p < 0.05$; ***$p < 0.01$; **** $p < 0.005$). (E–J) Representative brain sections of CA1 regions stained with the AT8 antibody and dentate gyrus region stained with the CP13 antibody. (K). Quantitative representation of percent hippocampal tissue stained (n=6) (*$p < 0.05$; **$p<0.01$; ***$p<0.005$). Statistical analyses were performed by

ANOVA followed by Tukey's multiple comparison test if $p < 0.05$. Results presented as means ± SEM.

Figure 5. Sucrose increased tau phosphorylation via a Cdk5-dependent mechanism
Biochemical analyses were conducted on whole brain homogenates from 8 mice/group. (A)
Representative Western blots probed with the indicated antibodies. (B–C) Relative protein
levels were quantified by densitometric analyses. The graphs were generated by normalizing
each protein of interest to β-Actin loading control (* $p < 0.05$). Statistical analyses were
performed by ANOVA followed by Tukey's multiple comparison test if $p < 0.05$. Results
presented as means ± SEM.